ChemCatChem

Research Article
doi.org/10.1002/cctc.202501112

Chemistry Europe
European Chemical Societies Publishing

www.chemcatchem.org

C-Acylation of Guaiacol with Acetic Acid Over Solid Acid Catalysts Under Mild Reaction Conditions

Nicola Schiaroli,*[a, b] Francesca Foschi,[a] Massimo Mella,*[a] and Carlo Lucarelli[a, b]

The direct acylation of substituted arenes by carboxylic acids offers a sustainable route to valorize biomass-derived aromatics, avoiding the use of more hazardous and high-impact reagents such as anhydrides or acyl chlorides. In this work, we study the liquid phase acylation of guaiacol (G) with acetic acid (AA) at 120 °C and atmospheric pressure, catalyzed by commercial Aquivion PW87 resin. This system yields 2-metoxyphenyl acetate (MPA) and 4-hydroxy-3-methoxyacetophenone (p-HMAP), valuable intermediates to produce fine chemicals. MPA is the primary kinetic product, but it is progressively consumed with simultaneous formation of HMAPs and G, indicating a sequential reaction pathway that favors the formation of p-HMAP with high regioselectivity (para/ortho-HMAP molar ratio of 26). Interestingly, from the mechanistic viewpoint and given the similar energetics of the two isomers, this finding can only be rationalized by invoking an intermolecular mechanism, rather than an intramolecular (or Fries) rearrangement. Electronic structure calculations were used to investigate pathways involving either MPA reacting with G to form HMAPs, or two MPAs yielding G and O-acylated acetophenones (minor products). The results suggest that the latter governs the acylation regioselectivity, with the key step being the acid-activated attack of the MPA ester on an aromatic ring, energetically favoring p-HMAP formation.

1. Introduction

Lignin, a major component of lignocellulosic biomass, represents a promising renewable source of aromatic compounds for the synthesis of fuels, polymers, and fine chemicals.[1–5] Recent advances in lignin depolymerization include pyrolysis, hydrogenolysis, and oxidative cleavage. [6–8] These approaches, allows for selective β—O—4 bond cleavage via thermochemical or catalytic route to obtain bio-oils containing a variety of monomeric phenolic such as guaiacol, syringol, and vanillin together with other oxygenated compounds such as aldehydes, carboxylic acids, and ketones.[9,10] Among them, 2-methoxyphenol (Guaiacol, G) is of particular interest due to its abundance, chemical versatility, and broad range of applications. [11] Techniques such as solvent extraction [12] and staged condensation [13] allow for its selective recovery from bio-oils, [14] enhancing its purity and enabling its use in the synthesis of fragrances,[15] pesticides,[16] and drugs.[17] In this regard, the acylation of G for the production of 2-methoxyphenyl acetate (MPA, used in the fragrance industry) and 4-hydroxy-3-methoxyacetophenone (HMAP, an hydroxy-aryl ketone), which is an active ingredient for many drugs with anti-asthma, anti-arthritis, and anti-atherosclerosis properties,[18,19] represents a desirable way to obtain high added value chemicals starting from abundant and cheap renewable sources (Scheme 1).

Catalytic acylations are traditionally carried out with highly reactive molecules such as anhydrides or acyl halides using Lewis acids ($AlCl_3$ and $ZnCl_2$), or strong Brønsted acids like H_2SO_4, posing significant issues related to their disposal and the high consumption of resources. Therefore, the substitution of these compounds with active and recyclable heterogeneous catalysts able to promote the reaction in mild reaction conditions is of paramount importance. Although different works have reported on the acylation of anisole, phenol, and toluene using acetic anhydride over different zeolites,[20–23] very few works regarding G acylation can be found in the literature.

The liquid phase acylation of G over a supported heteropoly-acid catalyst was studied by Yadav et al.[24] using 1,4 dioxane as a solvent. By investigating different acylating agents they found that, using vinyl acetate, it was possible to gain high G conversion (97%) at 170 °C, but no data regarding the products distribution were reported. Moreover, it was found that in these conditions, acetic acid (AA) was an ineffective acylating agent, leading to no G conversion when employed. In this respect, however, an efficient use of AA in the reaction would lead to highly desirable environmental benefits. In fact, AA can be produced via different green routes such as pyrolysis,[25,26] biogas, or methanol upgrading,[27–29] or biomass fermentation,[30] and, being widely employed in acetic anhydride manufacture, its direct use in organic syntheses would remove a rather energy-demanding step from the production chain. Nevertheless, the AA intrinsic

[a] N. Schiaroli, F. Foschi, M. Mella, C. Lucarelli
Dipartimento di Scienza e Alta Tecnologia, Università degli studi dell'Insubria, Via Valleggio 11, Como 22100, Italy
E-mail: nicola.schiaroli@uninsubria.it
massimo.mella@uninsubria.it

[b] N. Schiaroli, C. Lucarelli
Consorzio INSTM, Research Unit of Como, Via Giuseppe Giusti 9, Firenze 50121, Italy

Supporting information for this article is available on the WWW under https://doi.org/10.1002/cctc.202501112

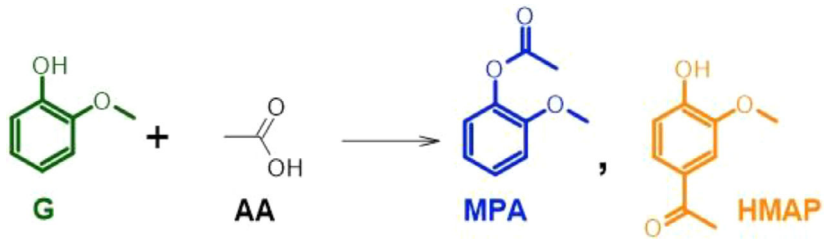

Scheme 1. Guaiacol acylation with acetic acid and possible products of reaction.

inefficiency in forming acylium ions, commonly believed to be involved in C-acylations, causes its activation to occur mainly in the gas phase, using acid catalysts at high temperature.[31–33] In this context, only a few recent works in the literature deal with G acylation using AA. HZSM-5 was found to efficiently catalyzed the gas phase reaction hitting a G conversion of 26.7% at 250 °C.[34] Regardless of the reaction conditions, the O-acylation was favored with MPA as the main product. Although HMAPs (different isomers of HMAP) were formed with yields of ≈ 7%, significant amounts of by-products such as catechol and its derivatives were formed (yields of 5% and 4%, respectively) through G demethylation and/or disproportion. In a later work, Gutiérrez-Rubio et al.[35] studied the gas phase reaction (270 °C) over different micro-, nanocrystalline and hierarchical ZSM-5 and Beta zeolites finding that, depending on the accessibility and the nature of the active sites (Lewis or Brønsted), it is possible to tune the selectivity of the reaction toward HMAPs formation. In this context, nano and -hierarchical ZSM-5 was able to better catalyze HMAPs production together with a significant presence of catechol and its acetates, which decreased during the time-on-stream due to catalyst deactivation. According to our best knowledge, studies concerning the catalytic acylation of G with AA under mild reaction conditions have not previously been reported in literature. Therefore, in this work, the liquid phase acetylation of G for the synthesis of MPA and HMAPs was investigating over an acidic Aquivion PW87 catalyst. The performance of this commercial perfluorosulfonic resin, classified as a superacid solid with high chemical and thermal resistance,[36] were studied in detail posing particular attention on the effects of the main reaction parameters on the reaction output. Motivated by the high regioselectivity toward the para isomer afforded by the ring-acylation process, electronic structure methods were employed to investigate possible reactive channels to find a mechanistic rationalization. Considering that the synthesis of hydroxy-aryl ketones is generally carried out in two steps involving the synthesis of the aryl ester followed by the Fries rearrangement of the substrate, the proposed one-step process represents a desirable and alternative synthetic approach to reduce the impacts associated with the traditional process.

2. Results and Discussion

2.1. Catalytic Activity–Effect of Water on Catalytic Performance

The catalytic activity of Aquivion PW87 at 120 °C as a function of the reaction time is shown in Figure 1. The conversion of G increased in the first 4 h of reaction, reaching a value of 13%, which remains constant with time. In these conditions, the formation of HMAP is highly unfavorable, and only a low yield of 3% is obtained after 6 h (Figure 1a). The main product of the reaction is MPA, which is produced with a selectivity of 86 % after 2 h (Figure 1b). Notably, this value decreased with reaction time (S_{MPA} = 56% after 6 h), whereas the HMAP selectivity increased, suggesting, in accordance with the constant G conversion, the occurrence of consecutive MPA reactions that led to HMAP formation.

At the same time, a notable formation of by-products (reported as "others") was observed (S_{others} = 18%). These compounds derived mainly from the hydrolysis of G and its subsequent O-acylation with AA to give mono- and poly-acylated compounds (Scheme 2 and Figure S1) whose overall yield was comparable to that of HMAP regardless of the reaction time. All in all, the presence of water, formed during acylation, led to the production of catechol (and "others" compounds) and shifted the reaction equilibrium toward the reagents, limiting both the conversion of G and the production of the desired compounds.

To improve catalyst efficiency and overcome the limitations imposed by the chemical equilibrium, a reaction vessel consisting of a separate dehydrating section, which continuously removes water vapor from the reaction environment, was implemented. In this section, water is adsorbed in the gas phase over a fixed bed composed of molecular sieve 3 Å pellets, while excess AA is refluxed back into solution (Figure S2). The same system can be successfully used to remove methanol from a dimethyl carbonate solution in a process called reactive vapor absorption (RVA).[37]

2.2. Catalyst Performance with Water Removal

The catalytic performance of the new reaction system as a function of the reaction temperature are reported in Figure 2a,b (reaction time of 6 h, AA/G molar ratio of 10). The removal of formed water from the reaction environment sensibly boosted the catalyst activity even in mild reaction conditions. G conversion at 100 °C reached a value of ≈ 13%, comparable to that obtained at 120 °C using the standard reactor configuration. In this test, MPA formation was favored (S_{MPA} = 89%) and a low production of HMAP was observed. At increasing reaction temperature, G conversion was enhanced up to a value of 27% at 120 °C together with HMAP and MPA yields (6% and 20%, respectively, after 6 h), whose selectivity values remained nearly

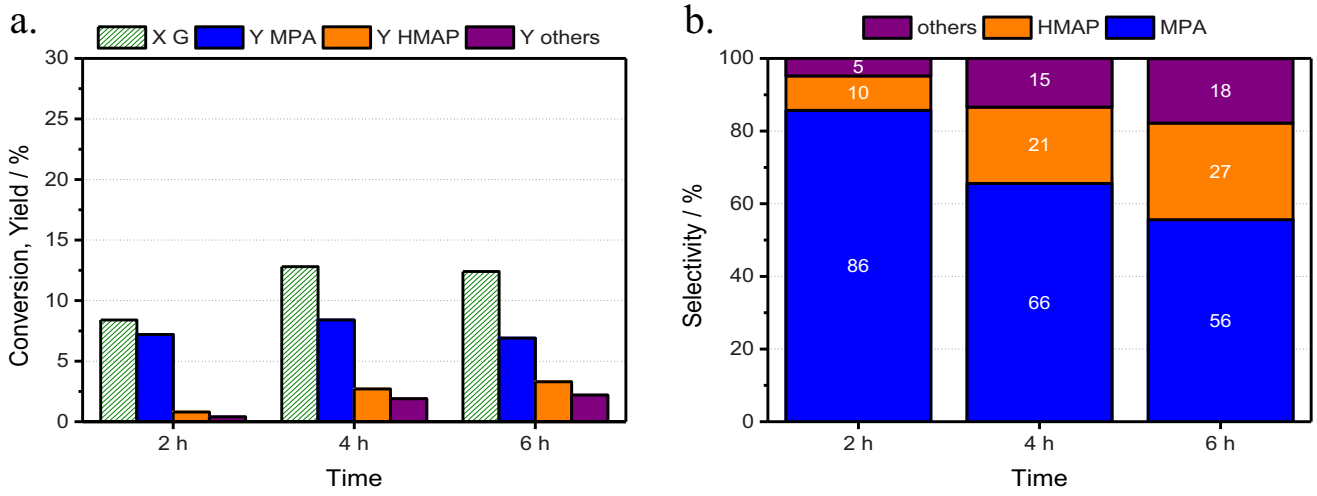

Figure 1. Catalytic activity of Aquivion PW87 at 120 °C without water removal as a function of the reaction time in terms of a) conversion and product yields, and b) selectivity. (AA/G: 10 mol/mol, 0.2 g of catalyst).

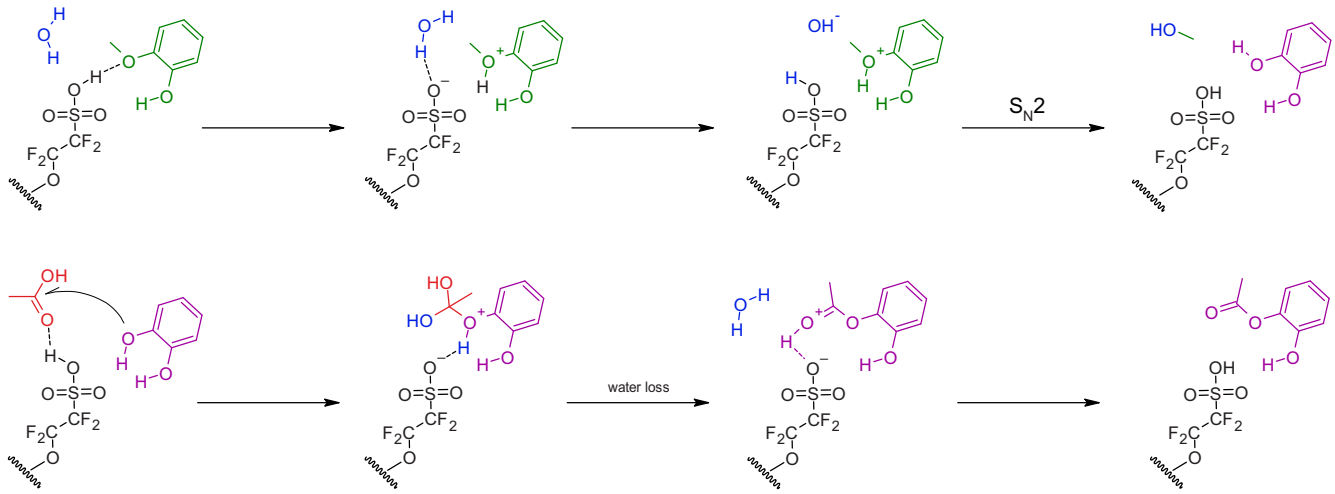

Scheme 2. Plausible reaction mechanism for the formation of the main by-products via G hydrolysis and O-acylation.

constant beyond 110 °C. The total selectivity toward by-products formation was low and almost stable regardless to the reaction time, with overall yields comparable to those observed without water removal (Table S1). In this case, however, these by-products are not associated to G hydrolysis and catechol formation but, in accordance with the reduced presence of water in the reaction environment, they arise mainly from consecutive O-acylation reactions on the formed HMAPs (Figures S3 and S4). Considering that the process reached maximum efficiency at 120 °C, this temperature was chosen as the optimal one to investigate the catalytic system deeper. By halving the amount of catalyst, and therefore that of the acidic sites in the reaction environment, it was possible to significantly favor the O-acylation (esterification) reaction toward the production of MPA, formed with a selectivity of 91% after 6 h (Figure 2c,d). In this condition, G conversion was slightly decreased to a value of 22%, while HMAP and by-products formation was almost negligible. Interestingly, the yield of MPA was almost independent from the amount of catalyst used ($Y_{MPA} \approx 20\%$), suggesting the achievement of the chemical equilibrium for the ester formation from G. The influence of the AA/G molar ratio on the catalytic performances is depicted in Figure 2e,f. The products distribution was mostly unaffected by an increase of the reagent molar ratio from 10 to 15. In this condition, in fact, an appreciable improvement of G conversion was not observed, while a slight increase of HMAP yield (from 6% to 7%) was detected. On the contrary, decreasing the amount of AA led to appreciable differences in the catalyst activity. While G conversion was lightly increased to a value of 29%, an evident reduction of MPA yield was observed ($Y_{MPA} = 14\%$) together with a lower HMAP production. A considerable carbon loss of 9% was detected which, considering the higher molar concentration of G and MPA in this condition, is likely due to an enhanced interaction between these molecules and catalyst active sites.

The FT-ATR analyses reported in Figure 3 show the spectra of the catalyst after 6 h as a function of the different AA/G molar ratio employed.

Regarding the pristine structure of the resin, the bands at 628, 968 and 1054 cm^{-1} are ascribable to the stretching of C—S

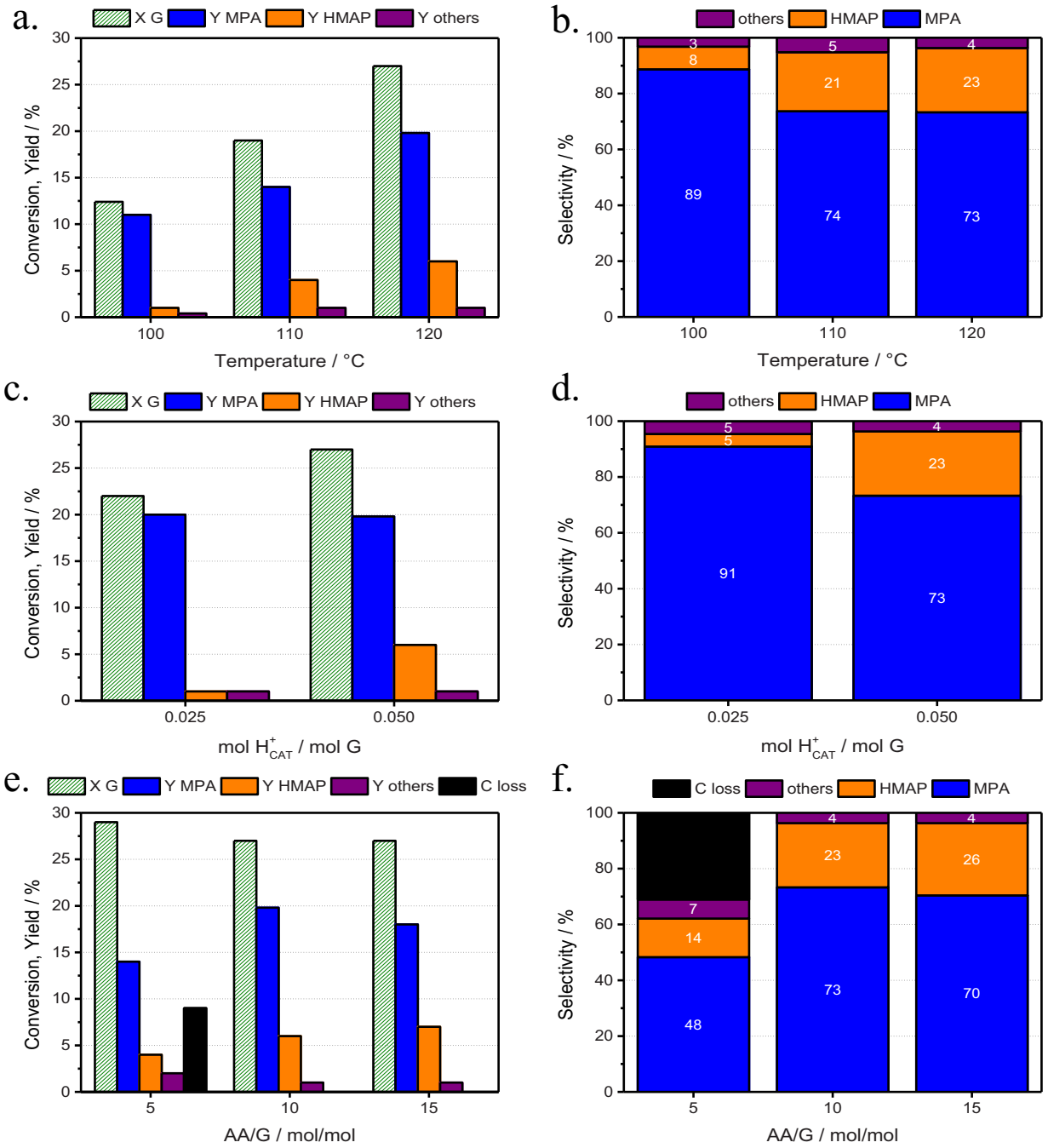

Figure 2. Catalytic activity of Aquivion PW87 at different operating conditions: a) and b) as a function of the reaction temperature (AA/G: 10 mol/mol, 0.2 g of catalyst, 6 h); c) and d) as a function of catalyst loading (120 °C, AA/G: 10 mol/mol, 6 h); e) and f) as a function of AA/G (120 °C, 0.2 g of catalyst, 6 h).

and both —SO_3H and C—O—C groups, respectively. The two peaks at 1150 and 1206 cm^{-1} are assigned to C—F stretching (symmetric and asymmetric) while the small bands between 1280 and 1320 cm^{-1} are due to asymmetrical S=O stretching. [39] At decreasing AA/G ratio, a series of additional bands appeared showing the formation of a carbonaceous layer over the catalyst surface. When the AA/G molar ratio was 10, it was possible to observe the presence of two main broad peaks centered at 1630 and 1559 cm^{-1} that can also be found even when the AA/G ratio was 5 and new bands around 1500 cm^{-1}, ascribable to C=O and-C=C- skeletal stretches,[38,39] were formed. In addition to these peaks, in the latter sample, bands at 1363, 1025 and 870 cm^{-1} appeared, ascribable to phenolic —OH stretching,[40] C—O vibrational stretching [41] and =C—H bending modes, respectively, suggesting a strong adsorption of G (or MPA and its derivatives) over the catalyst acidic sites.

The results reported in Figure 4a,b show the catalyst performance at 120 °C as a function of reaction time. G conversion increased only in the first 6 h, reaching a constant value of 27%, while HMAP was formed with a yield of 8% after 8 h of reac-

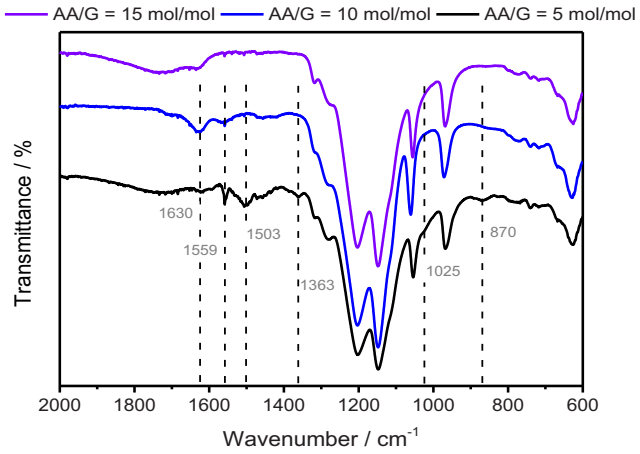

Figure 3. FT-ATR spectra of the catalysts after 6 h of reaction at 120 °C as a function of AA/G molar ratio.

tion. As the reaction time increased, a simultaneous decrease in MPA selectivity and a constant increase of HMAP production was observed. In details, after 6 h of reaction an intense decrease in MPA yield was observed which, in agreement with the constant conversion of G between 6 and 8 h, can be plausibly attributed to its consumption (MPA conversion of ≈ 34%) in favor of the formation of additional HMAP and heavy products, which led to a significant carbon loss after 8 h. Considering the MPA conversion in these last 2 h, a selectivity toward HMAP of 30% and to poly-acylated compounds (others) of 15% can be calculated. In agreement with the catalytic results, the FT-ATR spectra of the catalyst collected at different reaction times showed the progressive formation of a carbonaceous deposit on the surface of the resin (that turned from white to black during reaction), especially after 8 h (Figure 5).

At increasing reaction time, a series of broad additional bands in the 1350–1700 cm^{-1} region appeared. These peaks are similar to those previously observed for an AA/G ratio of 5 (Figure 3), suggesting a common coking mechanism between the different conditions tested. The possible deactivation of the catalyst was evaluated by reusing the Aquivion PW87 sample, after 6 h of reaction, in a second batch. After the washing of the resin with acetone and its further drying (at 120 °C for 12 h), the catalyst performances were evaluated after 6 h of reaction. The results depicted in Figure 6a show a sensible decrease in catalyst activity, which can be attributed to the presence of deactivating organic compounds over the surface of the resin. In detail, during the second reaction cycle, a G conversion of 20% and an MPA yield of 14% were observed, corresponding to a loss of activity of ≈ 30% compared to the first batch. Moreover, HMAP was produced in negligible amount while a carbon loss of 5% was detected, evidencing a further deactivation of the catalyst. As demonstrated in our previous work, [36] this resin can be easily and efficiently regenerated by treating the catalyst with a diluted nitric acid solution at 100 °C (20% in water, for 1 h) which, by oxidizing the carbonaceous deposit, restores the acidic active sites and thus the catalyst activity in further reaction cycles (Y_{HMAP} = 6% after regeneration, stable for three reaction/regeneration cycles).

The acylation of G with AA can be carried out over other acidic resins such as sulfonated polystyrene–divinylbenzene (SDVB) catalysts. This class of polymers can be used for catalyzing a wide range of organic reactions [42,43] but their activity depends on many factors such as the crosslinking degree (which determines their ability to swell and the specific surface area), the concentration of the acidic sites (typically expressed as mmol H^+/g), and the reaction environment. Figure 6b illustrates the performance obtained using Amberlyst-15 (a commercial resin, crosslinking degree of 20%, 4.70 mmol H^+/g) and a home-made 2%-SDVB catalyst (crosslinking degree of 2%, 5.00 mmol H^+/g). These solids, although being characterized by a higher concentration of acidic sites, showed results similar to those attained with Aquivion PW87 only in terms of HMAP yield. Though the highest G conversion was obtained with 2%-SDVB

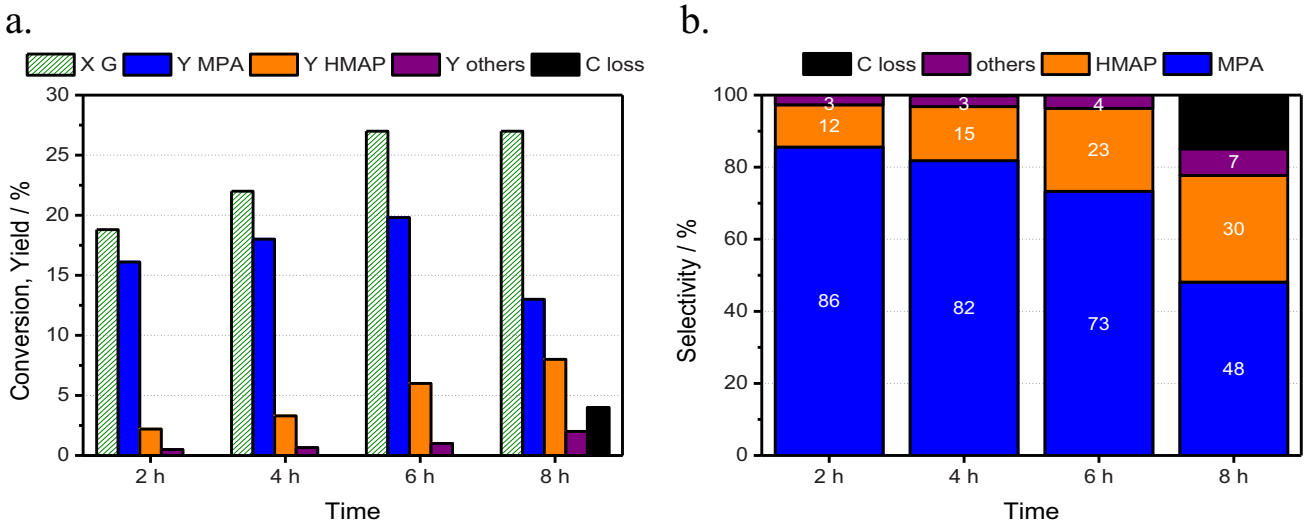

Figure 4. Aquivion PW87 activity as a function of reaction time in terms of a) Conversion and yield; b) Selectivity of the products (120 °C, AA/G: 10 mol/mol, 0.2 g of catalyst).

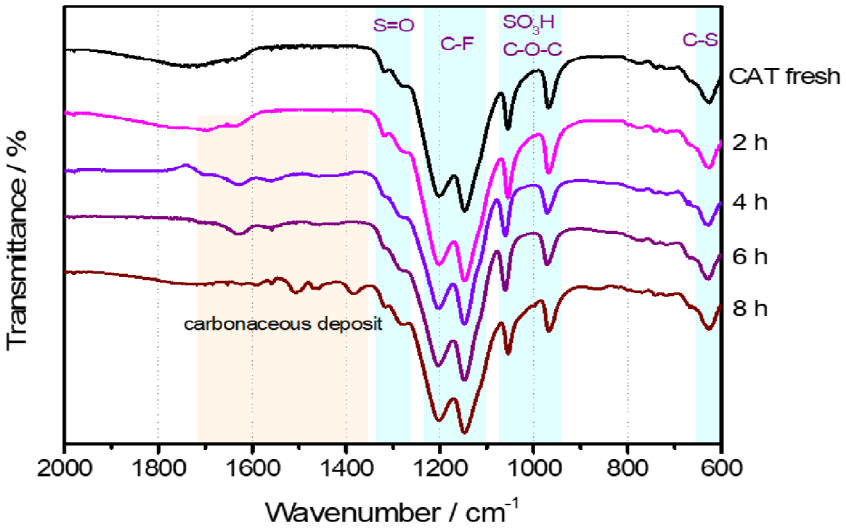

Figure 5. FT-ATR spectra of fresh and spent catalyst as a function of reaction time (120 °C, AA/G: 10 mol/mol, 0.2 g of catalyst).

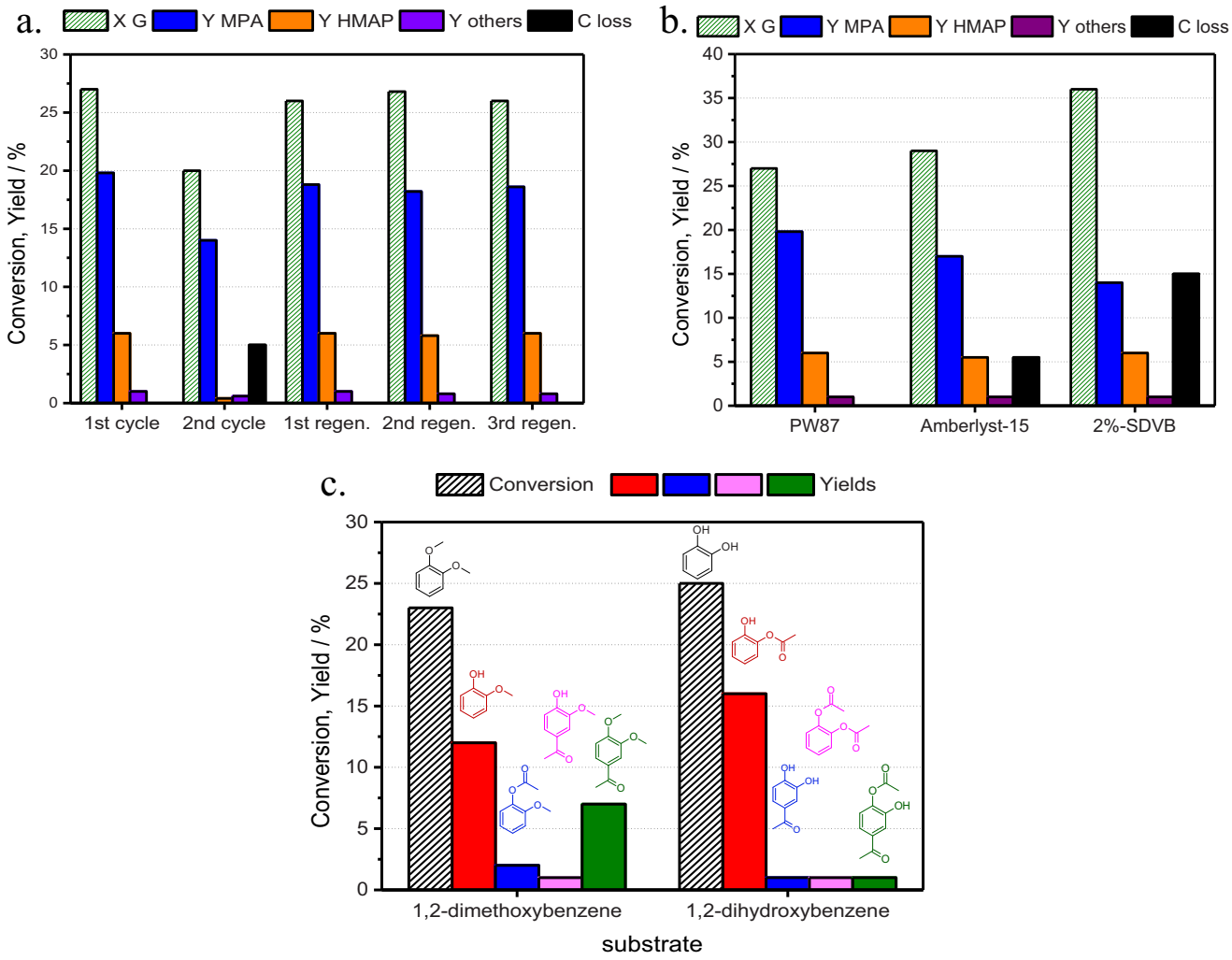

Figure 6. a) Catalytic activity of Aquivion PW87 in two cycles of reaction before and after regeneration; b) Comparison between activity of Aquivion PW87 and other solid acid catalysts in G acylation with AA; c) Catalytic results obtained using AA and 1,2-dimethoxybenzene or 1,2-dihydroxybenzene as substrate. (Reaction conditions: 120 °C, 0.2 g of catalyst, 6 h).

catalyst (X_G = 36%), this was associated with an extensive carbon loss of ≈ 15% which seems to be related to the consumption of MPA, produced with an extremely low selectivity (S_{MPA} = 39%). Similarly, Amberlyst-15 showed a significant carbon loss after 6 h of reaction together with a greater G conversion, but a yield in MPA lower than those obtainable with Aquivion PW87 which, combining a higher chemical inertness and a lower concentration of acidic sites (1.15 mmol H^+/g), seems to disfavor the formation of heavier compounds. It is noteworthy that the same catalytic system (and reaction setup) can be effectively applied to the C-acylation of 1,2-dimethoxybenzene (Figure 6c), a model compound in lignin valorization, under the optimized conditions identified for G acylation. In this case, a substrate conversion of 23% is associated with the formation of G (via hydrolysis) with a yield of 12% and the formation of 1-(3,4-dimethoxyphenyl)ethanone (yield of 7%), resulting from (para-)C-acylation of the substrate. Following G formation during the reaction, the presence of MPA and HMAP was also detected with yields of 2% and 1%, respectively. Conversely, performing the reaction with 1,2-dihydroxybenzene does not appear to favor C-acylation of the substrate, instead leading predominantly to the formation of 2-hydroxyphenil acetate (via O-acylation), with yields of only ~1% for all the other acylation products (see Figure S5 for further details).

2.3. Mechanistic Insights

The direct aromatic ring acylation with AA to form hydroxyacetophenones (HAPs) is generally carried out at temperatures higher than 200–250 °C. [31,32,34,44] In fact, only in these harsh conditions AA can act as a direct acylating agent, overcoming its low tendency to form acylium ions (or ketenes) notoriously involved in acylations. Conversely, the production of HAPs at mild reaction conditions can be achieved through the acid catalyzed rearrangement of phenolic esters (such as phenylacetate) in the liquid phase.[45,46] The two HAPs isomers (ortho- and para-HAP, namely o-HAP and p-HAP) are generally formed at the same time but they are assumed to derive from two different reaction pathways. The production of o-HAP is associated with an intramolecular rearrangement (Fries rearrangement) of the phenolic ester while the generation of p-HAP occurs via an intermolecular reaction.[47–49] In this context, from the analyses of the reaction mixture, by combining ^{1}H NMR and GC-MS techniques, it was possible to determine the regioselectivity of the reaction in HMAPs production in terms of 4-hydroxy-3-methoxyacetophenone (Apocynin, para-isomer, p-HMAP) and 2-hydroxy-3-methoxyacetophenone (ortho-isomer, o-HMAP). It was found that, in the tested conditions (120 °C, AA/G: 10 mol/mol) and independently from the reaction time, a nearly constant p-HMAP/o-HMAP molar ratio of 26 was obtained, corresponding to a p-HMAP purity of ≈ 96% of the HMAPs formed and to a selectivity value of 29% ($S_{p\text{-}HMAP}$) after 8 h of reaction (Figure S4). These values are far superior to those obtained in the literature (Table 1) regarding the acylation or the rearrangement of various aromatic compounds over acidic catalysts conducted in both gas or liquid phase (GP and LP, respectively). These results, together with the trends observed in the different catalytic tests, suggest that the formation of HMAP occurs predominantly through an intermolecular mechanism, which, together with the low temperature of reaction, favors the prevalent formation of the p-HMAP product over the o-HMAP isomer.

To further investigate the plausible reaction mechanism, an additional catalytic test was performed on Aquivion PW87 at 120 °C using MPA as a reagent with AA (AA/MPA: 10 mol/mol). As highlighted in Figure 7, MPA was found to be very reactive in these conditions, reaching a conversion value of 80% after 6 h. Interestingly, in this case, a remarkable yield in HMAP of 15% was observed together with the simultaneous formation of G in large quantities (Y_G = 51%), suggesting an intermolecular rearrangement in which the ester group of MPA acts as the effective (C-)acylating agent while G is the leaving group of the reaction intermediate.

As expected, a high p-HMAP/o-HMAP molar ratio of 20 was detected, which, besides being very close to that observed in the other catalytic tests, further corroborates the hypothesis of a mechanism involving an intermolecular rearrangement between the aromatic substrates. Moreover, although the reaction led to the production of a limited amounts of by-products (Y_{others} = 2%), a high carbon loss of 13% was detected, confirming the prevalent role of MPA in catalyst coking and deactivation. Based on these results it is possible to propose a plausible reaction mechanism involving the formation of all main products of reaction (Scheme 3). After the esterification reaction between G and AA (Reaction 1), the formed MPA can act as a C-acylating agent for both an activated G (producing HMAP, Reaction 2) and/or for another MPA molecule, generating G and 4-acetyl-2-methoxyphenyl acetate (AMPA, also detected in "others" products, Reaction 3 and Figure S3). Similarly to MPA, an acylium ion can be formed from AMPA activation, likely forming HMAP and MPA through its interaction with G (Reaction 4). In accordance with the catalytic results, the coking of the catalyst (and the detected carbon loss) is linked to the presence of MPA and/or to the enhanced production of HMAP (or AMPA), suggesting the occurrence of Reaction 5, responsible for the formation of highly reactive acylium ions (or ketene) able to interact with reaction environment and the catalyst surface forming heavier and deactivating compounds over the active sites of the resin.

2.4. Theoretical Modelling of Acylation Processes Mediated by MPA

2.4.1. General Energetic Considerations and Discussion on Explored Mechanistic Pathways

The large differences in the HMAP regio-isomer populations highlighted in Table 1, which also provides one with an appropriate literature comparison, and Figure 7 appear as the most interesting finding in needs of a complete mechanistic rationalization. For this reason, and for the sake of limiting the presentation of results with a somewhat lower interest, we discuss in this section of the main article the relevant energy profiles leading

Table 1. Literature review regarding the activity of different solid acid catalysts in the acylation or in the Fries rearrangement of aromatics in terms of hydroxy-aryl phenones yields (HAPs) and reaction stereoselectivity expressed as p-HAP/o-HAP molar ratio. "GP" and "LP" stand for gas phase and liquid phase, respectively.

Substate	*T*(°C)	p-HAP/o-HAP	Y HAPs (%)	Catalyst	Reference
Guaiacol and acetic acid	250 (GP)	2.2	58	HZSM-5	34
Guaiacol and acetic acid	270 (GP)	n.d.	9.0	HZSM-5	35
Phenyl acetate	250 (LP)	1.3	n.d.	H-Beta	49
Phenyl acetate	120 (LP)	2.3	1.5	Sulfated-SBA-15	45
Phenyl acetate	130 (LP)	0.8	1.3	$H_3PW_{12}O_{40}/SiO_2$	46
Phenyl acetate	150 (LP)	2.6	4.0	$H_3PW_{12}O_{40}$	50
Phenyl benzoate	130 (LP)	3.7	4.5	$H_3PW_{12}O_{40}$	50
Phenol and benzoic acid	200 (LP)	5.5	6.0	Sulfated Zirconia	51
Guaiacol and acetic acid	120 (LP)	26.0	6.0	Aquivion PW87	This work

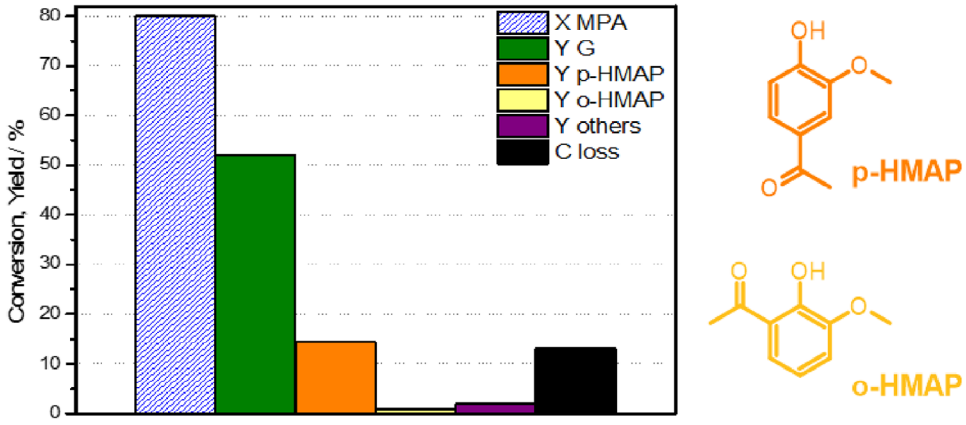

Figure 7. Catalytic results of MPA acylation with AA using Aquivion PW87 (200 mg). Reaction conditions: 120 °C, MPA = 5 mmol, AA = 50 mmol, 6 h of reaction.

from MPA to the two HMAP regio-isomers and confine the discussion of all other results in the Supporting Information. This notwithstanding, it is worth mentioning that:

1. other reaction paths have been explored to support the idea that the "MPA plus MPA to HMAP" channel is, de facto, the one correctly justifying the experimental outcomes (Figures S6–8).
2. The studied transformation is, substantially, under thermodynamic control, as ALL principal species involved (i.e., MPA, HMAPs, and AMPAs) lie above the reactants (AA and G), the sum of their energy being taken to define the zero of the energy scale. This finding itself already rationalizes the increase in G conversion and MPA/HMAP/AMPA production shown in Figure 2a upon increasing the temperature following 6 h of reaction. Albeit some extent of kinetic control may be present, at least on the relative product selectivity (e.g., *vide* Figure 4), the investigated transformation should, therefore, not be expected to reach complete G conversion unless parasitic reactions or products decomposition took place (vide infra for more discussion).
3. The esterification of G was found to be quite fast (21.2 kcal/mol of activation energy from the resin-adsorbed reactants, the TS being located at −4.1 kcal/mol below the energy zero due to the interaction between reactants and resin) compared to the subsequent transformations involving MPA (vide infra Figure 9). This characteristic may be used to rationalize the limited impact observed when lowering the catalyst amount on MPA production (Figure 2c) after 6 h of reaction as due to having reached a substantial thermodynamic equilibrium in both cases. Conversely, the slower kinetics of the MPA transformation leading to HMAP and AMPA is much facilitated by the higher quantity of acid sites (Figure 4a).

Apart from the experimental evidence involving the direct production of HMAP from MPA presented in the previous section (see Figure 7), additional indications that the transfer of the acetyl moiety may take place from the ester group to the aromatic ring are obtained comparing the relative energetics of the three AMPA regio-isomers obtained acylating MPA (4-acetyl-, 5-acetyl-, and 6-acetyl-2-methoxyphenyl acetate, respectively 4-, 5-, and 6-AMPA), and considering the energy changes associated to reaction 3 in Scheme 3. All these thermodynamic results are shown in Figure 8 together with the equilibrium structures of the AMPA compounds. From the latter, it is clearly apparent that 4-AMPA and 5-AMPA are substantially more stable (at least by 4.2 kcal/mol at the ZPE-corrected energy level) than 6-AMPA, the species from which o-HMAP would derive following de-esterification. Translating such energy differences in relative

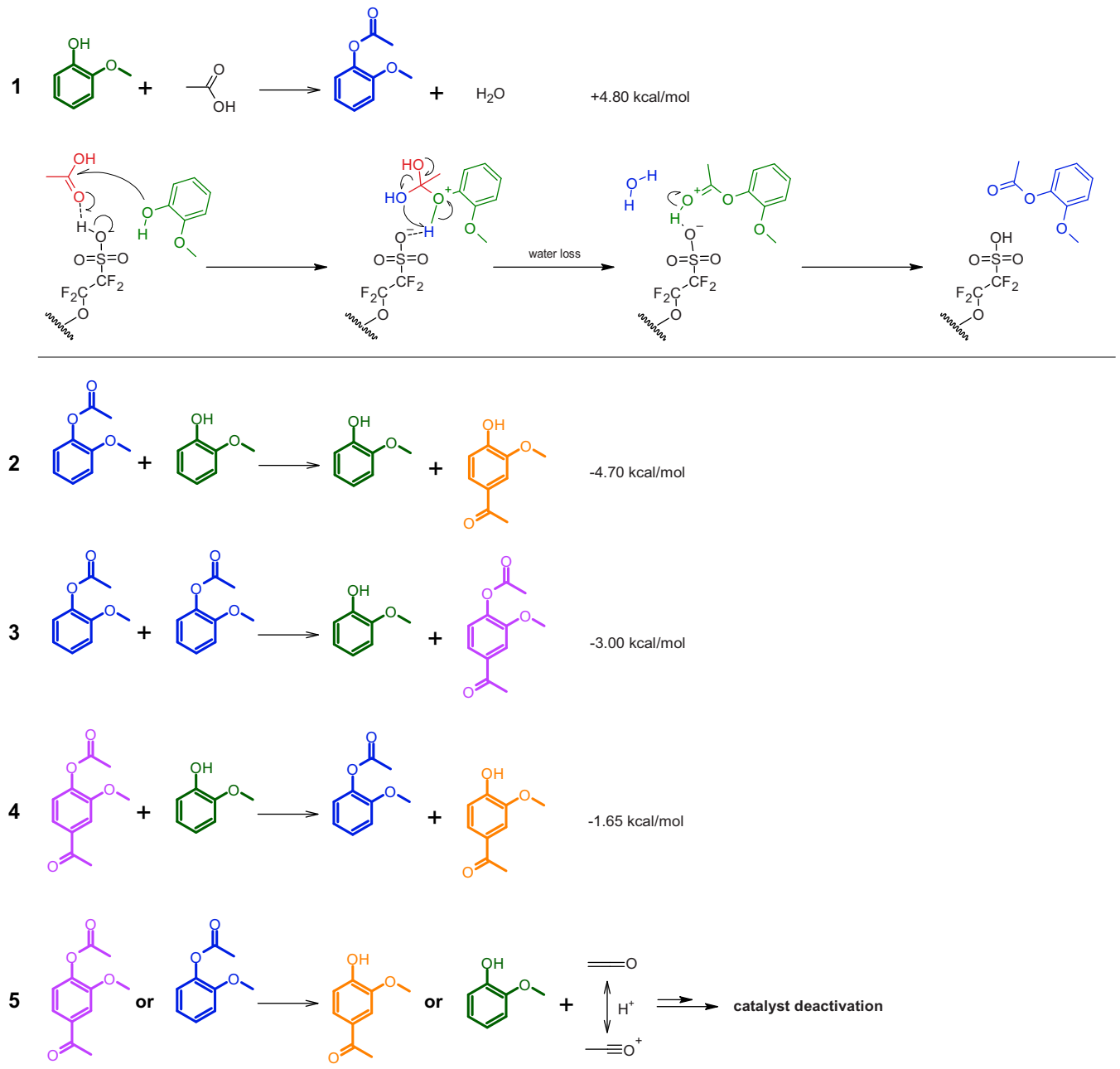

Scheme 3. Proposed reaction pathways involved in G acylation with AA in the tested conditions with relative ZPE corrected reaction energies. (■) G, (■) MPA, (■) HMAP, (■) AMPA. The plausible reaction mechanism of reaction 1 is also presented.

regioisomer population by assuming thermodynamic equilibrium suggests that a two hundredfold higher concentration of 4- and 5-AMPA should be present compared to the one of 6-AMPA. In principle, such a relative molar fraction may be sufficient to rationalize the experimental outcome of a preferential production of p-HMAP compared to o-HMAP. This result needs also to be contrasted with the relative stability of the o- and p-HMAP, which, in principle, favors the latter by 0.8 kcal/mol; such results would suggest only a threefold higher p-HMAP concentration (vide Figure 8 for the energetics and structural details). Indeed, the latter result seems to agree well with the outcome of the gas phase transformation reported in Table 1.

2.4.2. Energy Profile of the Electrophilic Attack by MPA onto the MPA Aromatic Ring

To simulate the reactive systems as close as possible, we have included in our atomistic model also the terminal sulfonic portion of the acidic resin, as indicated in the Experimental section. Apart from providing the system with a Brønsted acid group (i.e., capable of transferring a proton to catalyze the chemical transformations), it would also maintain it overall electroneutral, and it may act as proton acceptor (i.e., a Brønsted base) favoring the re-aromatization of the Wheland-like species if present in its anionic form.

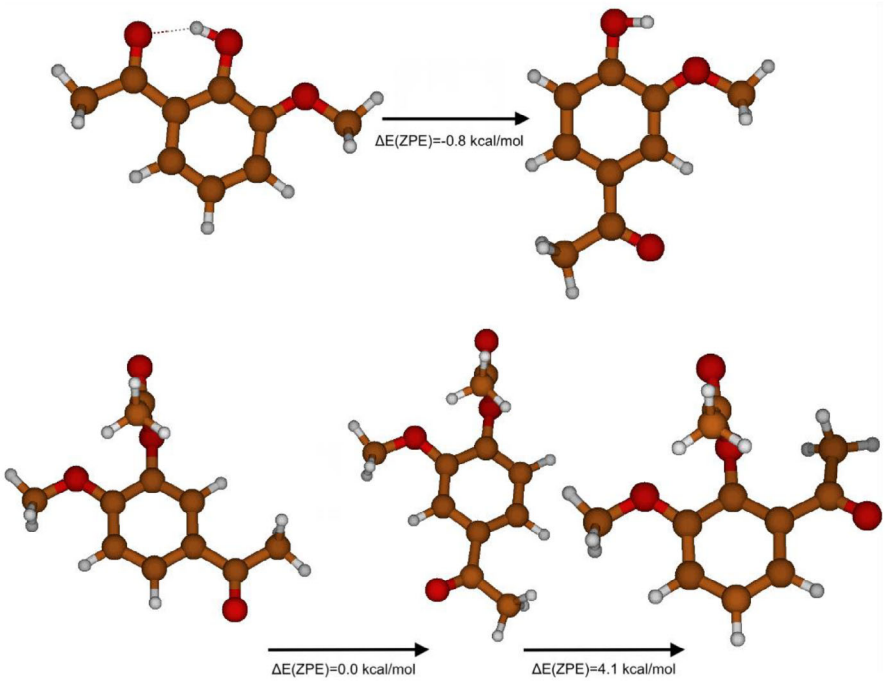

Figure 8. (Top) Relative energetics at the ZPE-corrected B3LYP/6–31++G(d,p) level for o- and p-HMAP (2-methoxy 6-acetyl and 2-methoxy 4-acetyl phenol). (Bottom) Relative energetics at the ZPE-corrected B3LYP/6–31++G(d,p) level for 5-AMPA, 4-AMPA, and 6-AMPA (2-methoxy 5-acetyl, 2-methoxy 4-acetyl phenyl, and 2-methoxy 6-acetyl acetate).

For each one of the two experimentally obtained regioisomers, we have investigated two possible paths potentially leading to each of them (Figure 9), assuming that the processes do not retrocede once either 4- or 6-AMPA are formed. Indeed, we found (vide infra Figure 10) that the overall process is thermodynamically spontaneous thanks to a sufficiently negative energy (or enthalpy) change, and that the paths differ only in the relative conformation/orientation of the two MPA molecules, as it can be appreciated in Figure 9. Interestingly, we have found that the most easily accessible transition state geometries display, invariably, a direct interaction between the sulfonate moiety and the hydrogen atom bound to the ring carbon receiving the electrophilic attack from the acid-activated phenyl acetate.

Apart from the obvious stabilization due to the electrostatic interaction between the anion and the Wheland-like species, the indicated structures also may have an unencumbered access to a direct path allowing the shift of the excess proton on the ring onto the sulfonate moiety with the simultaneous re-aromatization of the acylated ester. Indeed, the minimum energy path (MEP) from the shown TSs to the associated products has been found to lead, without barriers, to aromatic species following the spontaneous transfer of the proton to regenerate the sulfonic group. Besides, this idea also rationalizes the unsuccessful search for the TS of one of the conformers that may have led to the p-AMPA species, as the latter featured the excess proton on the ring pointing away from the sulfonate moiety; the lack of the electrostatic stabilization led, in fact, to putative structures, at least, 8 kcal/mol above the TS presenting the charged hydrogen bond.

As for the quantitative aspects of the ZPE-corrected energy profiles, we start mentioning that we defined as zero of the scale the energy of two isolated MPA species plus the fragment bearing the sulfonic moiety. From Figure 9, it is clear that the interaction between the latter and the two MPA molecules is, indeed, quite stabilizing (−18.4 and −21.3 kcal/mol for the path leading, respectively, to the o- and p-AMPA), and it is mediated by the formation of a hydrogen bond with the carbonylic group of a MPA, which consequently acts as the electrophilic reagent. The geometries in Figure 9 show that all ensuing TSs are, indeed, characterized by the sulfonic proton having been transferred to the electrophilic reagent, the bond between the latter and the phenyl ring of the second MPA being nearly formed.

As mentioned above, a hydrogen bond donated by the attacked phenyl ring to the sulfonate moiety by means of the hydrogen atom directly linked to the attacked carbon atom partially compensates for the charge separation in the TS and provides a substantial stabilization of the positive charge that may be borne by the ring itself. Importantly, the TS leading to p-AMPA appears to lie, at least, 6 kcal/mol below the most stable TS leading to the o-AMPA isomer. Given the similar relative disposition of the electrophilic reagent, of the attacked ring, and of the sulfonic moiety (i.e., of the hydrogen bonds stabilizing the structures), such a substantial difference ought to be related to the distance between the ester group on the attacked MPA and the resin fragment, their vicinity somewhat distorting the optimal structure that allows the TS leading toward p-HMAP to be better stabilized. In principle, such energy difference would already be sufficient to rationalize the experimental outcome for the larger amount of p-HMAP; a TS theory-based estimate,

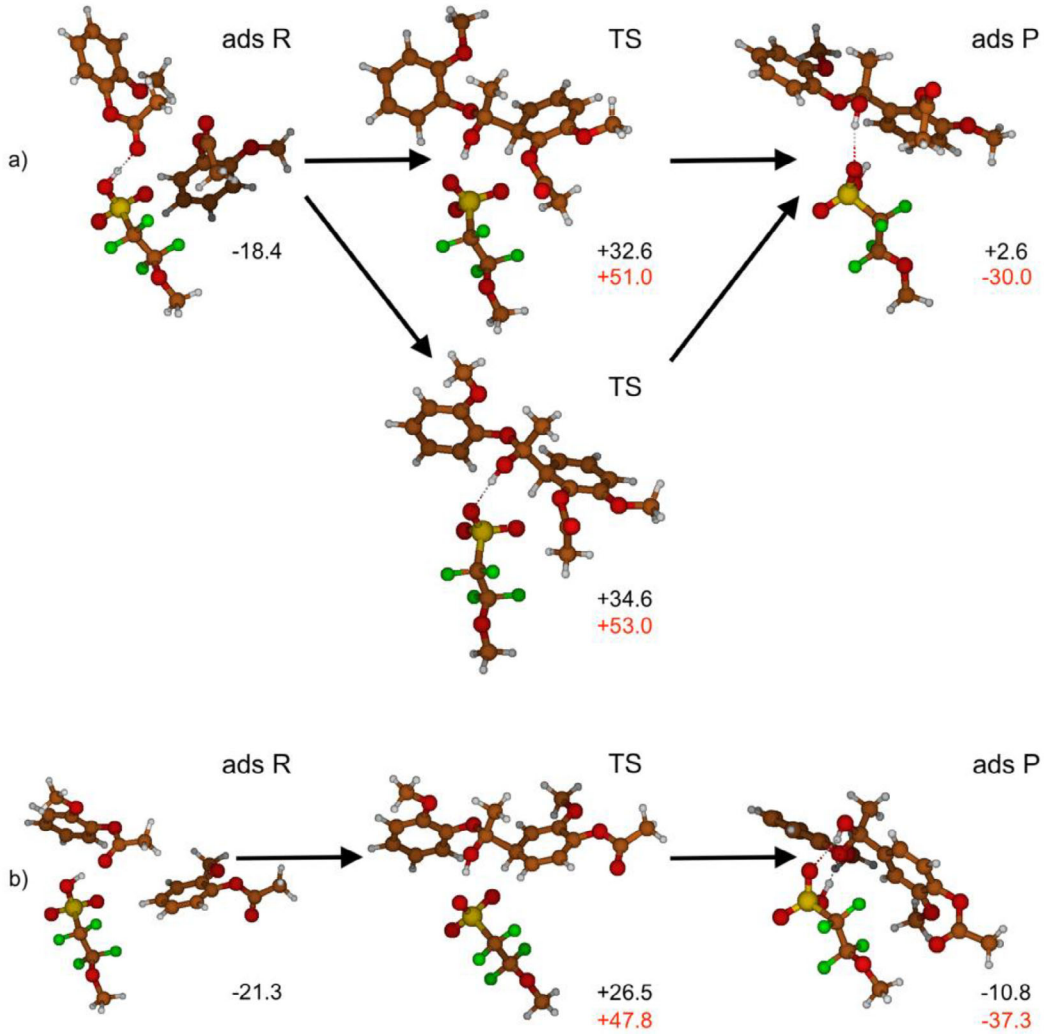

Figure 9. Attack of the acyl group on MPA on the phenolic ring of another ester. a) Path leading to the o-acylated ester; b) path leading to the p-acylated species. The energy profile, assuming as ZPE-corrected energy zero two isolated MPA and the resin model fragment, is indicated in kcal/mol using black colors; the difference in energy between a species and the following one along the path is, instead, indicated in red. Resin-adsorbed reactants (R) and products (P), as obtained following the minimum energy path, are indicated with the prefix "ads". The two TSs obtained for the o-acylation differ, primarily, due to the relative orientation of the phenyl ring of the attacking MPA; this explains the limited difference in energy.

[52] in fact, suggests that the discussed step alone may lead to a para/ortho ratio of, roughly, 2500. Indeed, the latter value appears to be quite high compared to the experimental outcome (26, see Table 1), or with the estimates based on relative energetics of the HMAP/AMPA isomers, and it may be due to the gas phase nature of the electronic structure calculations, which may exacerbate the impact of electrostatics compared to similar results for solubilized species.

To verify whether the absence of solvation effects may indeed have an impact, we recomputed TS barriers for the acylation process employing the PCM implicit solvent model, the energy difference between the TSs decreasing from 6.1 to 5.7 kcal/mol; the latter would suggest a lowering of the para/ortho ratio to a factor of 1500, roughly. In term of the barrier heights for the regioselective processes, these became 44.0 and 42.1 kcal/mol, respectively, for the o- and p-attack. In other words, the gas phase approximation appears to estimate barrier heights a few kcal/mol above what obtained when including solvation energetics by an implicit solvent model, a result suggesting that a change in the molecular charge distributions take place during the MPA attack to the ring so to make the TS more polar than the reactants. Even so, the relative energetics estimated in the gas phase appears sufficiently robust to draw useful conclusions on the mechanism albeit the absolute reactivity is somewhat depressed by using our chosen theory level. Obviously, the latter has its own implicit limitations due to the chosen DFT functional and basis set, which, unfortunately, cannot be easily improved due to the system size and large number of conformational isomers that must be explored to find a putative lowest energy path.

Apart from the computation difficulties just mentioned, endeavouring in such exercise may turn out to be unfruitful, as the overall experimental selectivity is likely to be influenced by other reactive processes involving subsequent reactivity of the products; these would preferentially consume the most rapidly produced regioisomer lowering the effective selectivity. This can

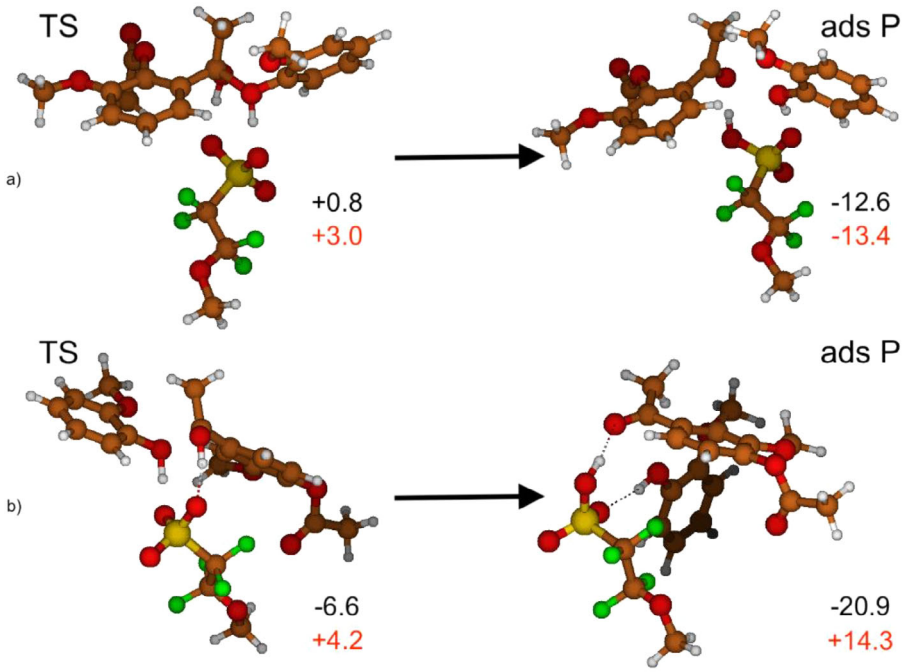

Figure 10. Elimination of G from the hemiketal obtained from the acylation of MPA due to the electrophilic attack of another ester. a) Path leading to the o-acylated ester; b) path leading to the p-acylated species. The energy profile, assuming as ZPE-corrected energy zero two isolated MPA and the resin model fragment, is indicated in kcal/mol using black colors; the difference in energy between a species and the following one along the path is, instead, indicated in red. Resin-adsorbed reactants (R) and products (P), as obtained following the minimum energy path, are indicated with the prefix "ads". The picture represents the TS resulting from the hemiketal obtained via o-acylation and following the conformational change leading to the formation of a direct hydrogen bond between the sulfonic group and phenolic oxygen atom.

happen, for instance, via carbon-loss processes, one of which is discussed in the following as a natural consequence of the mechanism we have proposed, and it involves the hemiketals produced by the first step in the ring acylation. In conclusion, the estimated selectivity ought to be considered simply representative of a relative kinetic preference toward p- AMPA and, consequently, p-HMAP due to the energy profile of the electrophilic acylation.

As a final comment on the first reactive step, we notice that the results just discussed make evident that, instead of a Wheland-like intermediate, the acylation reaction proceeds directly to form a hemiketal involving the o-methoxyphenate moiety in lieu of the more common alcoholic residue, in this way directly exploiting the possibility of an opposite charge recombination upon proton shift from the benzenium cation to the sulfonate anion. Consequently, the step just discusses qualitatively deviates from what commonly expected from electrophilic substitution on aromatic species.

2.4.3. Hemiketal Decomposition and AMPA Formation

As logical subsequent step in the investigated process, we turn to the elimination of o-methoxyphenol from the hemiketals, which may also require the involvement of the sulfonic group to activate the former as leaving group. For this, we could exploit the fact that the kinetic product obtained relaxing the TS structure leading to p-acylated MPA already presents the proton on the sulfonic group hydrogen bonded to the phenolic oxygen. Conversely, the o-acylated counterpart requires, in principle, an additional step involving a conformational change to properly orient for the activation of the leaving group, as it has the acidic proton interacting directly with the aromatic p-system. A set of constrained optimizations leading toward the o-substituted conformer with a hydrogen bond between the sulfonic group and the phenolic oxygen led to an energy lowering of −4.8 kcal/mol and suggested, also, that only a very low barrier (around 0.5 kcal/mol) should be present between the two species. Thus, reaching the required conformation appears to be controlled more by entropic factors than by energetic ones.

Figure 10 provides a pictorial representation of the species and energetics involved in the phenol elimination from the hemiketal species. As often, putative TS structures were obtained via constrained optimization while shortening the sulfonic proton–phenolic oxygen distance. Importantly, the energetic location of the elimination TSs is much lower than the one for the electrophilic substitution in all cases, so that the latter is clearly the kinetic bottleneck of the overall process. This notwithstanding, it is apparent that the pathway leading to the p-AMPA remains more facile also for the elimination step, the TS for the latter being 7.4 kcal/mol lower than the one leading to the o-AMPA product. This notwithstanding, the overall process leading to AMPA isomers appears thermodynamically favorable, at least when considering the latter and the produced G still interacting with the resin fragment.

In order to allow the sulfonic moiety in the latter to exert its catalytic activity, AMPA isomers should desorb; this process is predicted to require 6.3 and 10.6 kcal/mol for the ortho and para species and would leave, guaiacol bonded to the sulfonic

group via a donated hydrogen bond. The acidic proton would, therefore, remain available to interact either with the carbonyl of AA activating it for the esterification of guaiacol (*vide* Figure S7 and associated discussion in the Supporting Information), or with a MPA molecule reinitiating the catalytic process producing AMPAs. The latter could also be produced via the reaction:

$$\text{AMPA} + \text{MPA} \rightarrow \text{HMAP} + \text{AMPA}$$

which would convert into the desired product with the same associated energy change as the one for Reaction 2 in Scheme 3. Importantly, the abovementioned process is likely to maintain a high selectivity toward the para isomer of AMPA for the same set of reasons provided for Reaction 3 in Scheme 3. A similar outcome is also reached via Reaction 4, which would regenerate a HMAP molecule from AMPA and G.

2.4.4. Interpretation of Additional Experimental Outcomes

With a putative mechanism qualitatively rationalizing the p-AMPA/o-AMPA (or p-HMAP/o-HMAP) selectivity, we are well equipped to discuss additional experimental observations of general relevance. In this respect, we notice that both hemiketal species may produce substituted benzyl-type carbocations following acid-catalyzed loss of water, which may lead to the formation of a sulfonic ester (de facto, a ketal involving guaiacol, the sulfonic resin, and the ketonic group of 2-methoxy 6-acetyl phenyl acetate), or of an olefin (a styrene derivate) following the transfer of a proton from the methyl group to the sulfonate. Both these heavier compounds may act as alkylating agents for the aromatic MPA, HMAPs, and AMPA, eventually leading to carbon loss and deactivation of the resin catalytic properties indicated in the experimental section. In this respect, the coking mechanism just presented fits remarkably well with the experimental evidence provided in Figures 2, 4, and 6. In fact,

1. The decrease in carbon loss upon increasing the AA/G ratio shown in panel e and f of Figure 2 could easily be ascribed to both a dilution effect and the possibility that AA, acting as nucleophile, may limit the formation of either the benzylic carbocation or the substituted styrene, thus hurdling their attack to other aromatic species.
2. The increase in carbon loss upon increasing the reaction time after having reached maximum conversion (see Figure 4) may be easily interpreted as due to the production of secondary kinetic compounds, more strongly adsorbing onto the resin due to their multi-functional nature and higher mass, subsequently activated toward the attack on G, MPA, and HMAP. As for this, it is important to notice that our computational results suggest a near degeneracy between the adsorbed hemiketal formed following a para substitution of MPA and the final p-HMAP and G product, thus indicating only a limited thermodynamic driving force for this latter step. In other words, the hemiketal species may be able to remain adsorbed on the resin for a sufficiently long time to be activated toward the production of polyaromatic compounds. Obviously, this idea also rationalizes the increased carbon loss obtained upon reusing the resin without regenerating it with diluted nitric acid.
3. The higher carbon loss recorded while using styrene/divinylbenzene based resins compared to Aquivion PW87 is easily ascribed to the aromatic nature of the former matrices, which are naturally prone to be electrophilically substituted despite their conceivable deactivation due to the inductive -I effect of the sulfonic group. Whether due to their direct acylation by MPA, or because attacked by the abovementioned carbocation species, the net effect would be to consume part of the reactants for side processes likely to produce heavier polyaromatic compounds.

3. Conclusions

This study provides a few insights into the regioselective C-acylation of guaiacol with acetic acid under mild conditions, enabled by the use of a reusable Aquivion PW87 as solid acid catalyst. The high para-selectivity observed in optimized conditions, reaching a para/ortho ratio up to 26 mol/mol and a p-HMAP purity of 96%, substantially exceeds values reported for both gas- and liquid-phase systems in the literature. Importantly, this behavior is shown to stem not from classical intramolecular Fries-type rearrangements, but from an intermolecular mechanism involving MPA as effective acylating agent. Experimental and theoretical analyses converge in identifying key features responsible for this selectivity. DFT modelling reveals that sulfonate-mediated transition states stabilize the pathway associated with p-HMAP formation significantly more than the ortho-alternative, leading to a predicted selectivity that, besides being fully consistent with experimental data, is much higher than expected from thermodynamic considerations alone. These findings not only demonstrate how regioselectivity can be controlled at low temperature through intermolecular ester chemistry but also shed light on the deactivation phenomena observed. In fact, in this context, the formation of hemiketals and benzyl-type cations from AMPAs and HMAPs intermediates provides a plausible explanation for carbon loss and catalyst fouling observed with increasing reaction time and under conditions favoring HMAPs formation.

4. Experimental Section

4.1. Catalytic Tests

Aquivion PW87 (1.15 mmol H^+/g), Amberlyst-15 (4.70 mmolH^+/g), guaiacol, acetic acid, 2-methoxyphenyl acetate and 4-hydroxy-3-methoxyacetophenone were purchased from Sigma Aldrich, Polystyrene-divinylbenzene 2% crosslinked (2%-SDVB) 200–400 mesh was purchased from Alfa Aesar. While PW87 were used without any other treatment, Amberlyst particles were first crushed using an agata mortar prior to the tests. The sulfonation of 2%-SDVB resin was carried out according to our previous work. [36] The acylation of guaiacol with acetic acid was carried out in a 10 mL two-neck round flask reactor equipped with a reflux system (condenser) and a thermometer, the tests were performed at atmospheric pressure. When the dehydrating section was used, it consisted of a porous

quartz septum filled with 0.75 g of molecular sieve 3 Å in the form of pellets. This section was placed between the top of the reactor and the neck of the condenser. In a typical experiment, 5 mmol of guaiacol, the desired amount of acetic acid (25, 50 or 75 mmol) and catalyst (100 or 200 mg) were placed into the reaction system. The mixture was then stirred at 600 rpm and heated up to the desired temperature (100, 110 or 120 °C) in an oil bath. Then, the mixture was maintained at the set temperature for the desired reaction time (from 2–8 h). At the end of the experiment, the reaction system was quenched using an ice-bath and the reaction mixture analyzed using a GC (Autosystem XL, Perkin Elmer) equipped with a DB-5 column and a FID detector. The sample was prepared by diluting 200 µL of the reaction mixture with acetone and using octane as internal standard. The G conversion and MPA, HMAP and "others" selectivity and yields were calculated through the following equations:

$$\text{Conversion}: X_G = [(\text{molG}_{t0} - \text{molG}_{t1})/\text{molGt}_0]\text{x}100 \quad (1)$$

$$\text{Yield}: Y_{\text{MPA,HMAP,others}} = (\text{mol}_{\text{MPA,HMAP,others}}/\text{molG}_0)\text{x}100 \quad (2)$$

$$\text{Selectivity}: S_{\text{MPA,HMAP,others}} = \left[\text{mol}_{\text{MPA,HMAP,others}} / (\text{molG}_{t0} - \text{molG}_{t1})\right] \text{x}100 \quad (3)$$

$$\text{Carbonloss}: \quad 100 - [100\text{x}(\text{mol}_{\text{MPA}} + \text{mol}_{\text{HMAP}} + \text{mol}_{\text{others}} + \text{molG}_{t1}) / \text{molG}_{t0}] \quad (4)$$

where t0 is "before reaction" and t1 is "after reaction".

4.2. Characterization Techniques

The IR spectra of the catalysts before and after reaction were carried out in attenuated total reflectance (ATR) over the 4000–600 cm^{-1} range using a Thermo Scientific Nicolet iS10 Smart iTR equipped with a Smart OMNI Transmission instrument, interfaced with a Omnic 9.2.98 software. GC-MS analyses were performed in a Finnigan Trace GC-MS equipped with a DB-5 column and a quadrupole analyzer and electronic impact source. ^{1}H spectra were recorded on a Bruker Avance 400 (400 and 101 MHz, respectively); chemical shifts are indicated in parts per million downfield from $SiMe_4$, using the residual proton ($CHCl_3$ = 7.26 ppm) solvent resonances as internal reference. Coupling constants values *J* are given in Hz. The sample was about 8–10 mg.

4.3. Electronic Structure Modelling of the Catalytic Mechanism

Putative reaction paths for the formation of o- and p-HMAP from the reaction mixture have been explored employing electronic structure calculations at the B3LYP/6–31++g(d,p) level of theory [53] as implemented in the Gaussian09 suite of codes.[54] The level chosen for the purpose has been previously demonstrated to be valid in different circumstances involving the reactivity of organic compounds, even when the latter is acid/base catalyzed. Given the relatively low value of the electric permittivity of liquid acetic acid (AA, e_r = 6.17), we have chosen to explore all paths as if the reactions took place in vacuum; we have verified the validity of such approach occasionally testing for changes in the relative energetics obtaining uninfluential modifications of barrier heights and thermodynamics. As for the atomistic representation of the reactive systems, we have chosen to model the active functional groups in Aquivion PW87 as a freely moving fragment, namely 2-methoxy 1,1–2,2-tetrafluoro ethyl sulphonic acid. All the remaining species potentially involved in HMAP production have, instead, been modelled including all atomistic details. Putative structures for both energy minima and transition states (TSs) have been fully optimized and characterized computing the full hessian matrix of the potential energy surface (PES) followed by its diagonalization. Normal modes associated to negative curvatures of the PES at stationary points have been used to verify the atomistic details of the processes involved in the reactive steps.

Acknowledgments

The author has nothing to report.

Open access publishing facilitated by Universita degli Studi dell'Insubria, as part of the Wiley - CRUI-CARE agreement.

Conflict of Interests

The authors declare no conflict of interest.

Data Availability Statement

The data that support the findings of this study are available from the corresponding author upon reasonable request.

Keywords: Acylation · Aquivion · Density functional calculations · Heterogeneous catalysis · Reaction mechanisms

[1] X. Hu, M. Gholizadeh, *Renew. Sust. Energ. Rev.* **2020**, *134*, 110124.
[2] H. A. Baloch, S. Nizamuddin, M. T. H. Siddiqui, S. Riaz, A. S. Jatoi, D. K. Dumbre, N. M. Mubarak, M. P. Srinivasan, G. J. Griffin, *J. Environ. Chem. Eng.* **2018**, *6*, 5101–5118.
[3] A. Llevot, E. Grau, S. Carlotti, S. Grelier, H. Cramail, *Macromol. Rapid Commun.* **2015**, *37*, 9–28.
[4] D. M. d. A. Fragoso, F. P. Bouxin, J. R. D. Montgomery, N. J. Westwood, S. D. Jackson, *Technol. Rep.* **2020**, *9*, 100400.
[5] H. Wang, Y. Pu, A. Ragauskas, B. Yang, *Bioresour. Technol.* **2019**, *271*, 449–461.
[6] D. Chen, K. Cen, X. Zhuang, Z. Gan, J. Zhou, Y. Zhang, H. Zhang, *Combust* **2022**, *242*, 112142.
[7] M. Carrier, M. Windt, B. Ziegler, J. Appelt, B. Saake, D. Meier, A. Bridgwater, *Chem. Sus. Chem.* **2017**, *10*, 3212–3224.
[8] A. Das, A. Rahimi, A. Ulbrich, M. Alherech, A. H. Motagamwala, A. Bhalla, L. da Costa Sousa, V. Balan, J. A. Dumesic, E. L. Hegg, B. E. Dale, J. Ralph, J. J. Coon, S. S. Stahl, *ACS. Sus. Chem. Eng.* **2018**, *6*, 3367–3374.
[9] Y. Yin, C. Suo, C. Ma, S. Liu, *J. Environ. Chem. Eng.* **2025**, *13*, 116321.
[10] S. Karagöz, T. Bhaskar, A. Muto, Y. Sakata, *Fuel* **2005**, *84* 875-884.
[11] P. V. B. Bonjour, P. H. R. Alijó, M. L. L. Paredes, *Biomass Bioenergy* **2025**, *203*, 108227.
[12] G. Guo, Q. Huang, F. Jin, Q. Wang, Q. Fu, Y. Liu, Y. Chen, J. Wang, J. Zhang, *Fuel Process. Technol.* **2022**, *230*, 107216.
[13] S. Papari, K. Hawboldt, P. Fransham, *Fuel* **2019**, *245*, 233-239.
[14] S. Ma, L. Zhang, L. Zhu, X. Zhu, *J. Anal. Appl. Pyrolysis* **2018**, *131*, 113–119.
[15] K. Li, J. W. Frost, *J. Am. Chem. Soc.* **1998**, *120* 10545–10546.
[16] L. Yang, W. Zhou, K. Seshan, Y. Li, *J. Mol. Catal. A Chem.* **2013**, *368-369*, 61–65.
[17] S. L. Bhanawase, G. D. Yadav, *Catal. Today* **2017**, *291*, 213–222.
[18] E. van Den Worm, C. J. Beukelman, A. J. J. Van Den Berg, B. H. Kroes, R. P. Labadie, H. van Dijk, *Eur. J. Pharmacol.* **2001**, *433*, 225–230.
[19] S. R. Savla, A. P. Laddha, Y. A. Kulkarni, *Drug. Metab. Rev.* **2021**, *53*, 542–562.

[20] D. Rohan, C. Canaff, E. Fromentin, M. Guisnet, *J. Catal.* **1998**, *177*, 296–305.
[21] K. Smith, G. A. El-Hiti, A. J. Jayne, M. Butters, *Org. Biomol. Chem.* **2003**, *1*, 1560–1564.
[22] P. Botella, A. Corma, J. M. López-Nieto, S. Valencia, R. Jacquot, *J. Catal.* **2000**, *195*, 161–168.
[23] S. P. Chavan, R. Anand, K. Pasupathy, B. S. Rao, *Green Chem.* **2001**, *3*, 320–322.
[24] G. Yadav, A. Yadav, *Ind. Eng. Chem. Res.* **2013**, *52*, 10627–10636.
[25] T. Sarchami, N. Batta, F. Berruti, *Biofuel Bioprod. Biorefin.* **2021**, *15*, 1912–1937.
[26] J. De Maron, L. Bellotti, A. Baldelli, A. Fasolini, N. Schiaroli, C. Lucarelli, F. Cavani, T. Tabanelli, *Sustain. Chem.* **2022**, *3*, 58–75.
[27] N. Schiaroli, L. Negahdar, M. Lützen, P. Hoang Ho, L. J. Allen, A. Natoli, F. Ospitali, F. Maluta, E. Rodríguez-Castellón, C. D. Damsgaard, G. Fornasari, A. M. Beale, P. Benito, *J. Catal.* **2023**, *424*, 140–151.
[28] N. Schiaroli, M. Battisti, P. Benito, G. Fornasari, A. G. Di Gisi, C. Lucarelli, A. Vaccari, *Catalysts* **2022**, *12*, 109.
[29] J. L. Martín-Espejo, J. Gandara-Loe, J. A. Odriozola, T. R. Reina, L. Pastor-Pérez, *Sci. Total Environ.* **2022**, *840*, 156663.
[30] Y. Li, D. He, D. Niu, Y. Zhao, *Bioprocess Biosyst. Eng.* **2015**, *38*, 863–869.
[31] M. Guisnet, D. B. Lukyanov, F. Jayat, P. Magnoux, I. Neves, *Ind. Eng. Chem. Res.* **1995**, *34*, 1624–1629.
[32] C. L. Padró, C. R. Apesteguía, *J. Catal.* **2004**, *226*, 308–320.
[33] S. Gutiérrez-Rubio, I. Moreno, D. P. Serrano, J. M. Coronado, *ACS Omega* **2019**, *4*, 21516–21528.
[34] M. K. Montañez Valencia, C. L. Padró, M. E. Sad, *Appl. Catal. B Environ.* **2020**, *278*, 119317.
[35] S. Gutiérrez-Rubio, M. Shamzhy, J. Čejka, D. P. Serrano, I. Moreno, J. M. Coronado, *Appl. Catal. B Environ.* **2021**, *285*, 119826.
[36] N. Schiaroli, A. Allegri, M. Eberle, S. Billi, A. Guerrini, S. Albonetti, A. Vaccari, T. Tabanelli, C. Lucarelli, *ChemSusChem* **2023**, *16*, e202300903.
[37] T. Tabanelli, S. Cailotto, J. Strachan, A. F. Masters, T. Maschmeyer, A. Perosa, F. Cavani, *Catal. Sci. Technol.* **2018**, *8*, 1971–1980.
[38] L. Zhang, Z. Wu, N. C. Nelson, A. D. Sadow, I. I. Slowing, S. H. Overbury, *ACS Catal.* **2015**, *5*, 6426–6435.
[39] M. E. Potter, S. Mediavilla Madrigal, E. Campbell, L. J. Allen, U. Vyas, S. Parry, A. García-Zaragova, L. M. Martínez-Prieto, P. Oña-Burgos, M. Lützen, C. D. Damsgaard, E. Rodríguez-Castellón, N. Schiaroli, G. Fornasari, P. Benito, A. M. Beale, *Angew. Chem. Int. Ed.* **2023**, *62*, e202312645.
[40] E. Fuente, J. A. Menéndez, M. A. Díez, D. Suárez, M. A. Montes-Morán, *J. Phys. Chem. B* **2003**, *107*, 6350–6359.
[41] S. Jia, B. J. Cox, X. Guo, C. Zhang, J. G. Ekerdt, *Ind. Eng. Chem. Res.* **2011**, *50*, 849–855.
[42] N. Boz, J. G. Degirmenbasi, D. M. Kalyon, *Appl. Catal. B Environ.* **2015**, *165*, 723–730.
[43] M. Musolino, M. J. Ginés-Molina, R. Moreno-Tost, F. Aricò, *ACS Sus. Chem. Eng.* **2019**, *7*, 10221–10226.
[44] H. K. Chau, D. E. Resasco, P. Do, S. P. Crossley, *J. Catal.* **2022**, *406*, 48–55.
[45] R. van Grieken, J. A. Melero, G. Morales, *Appl. Catal. A Gen.* **2005**, *298*, 143–152.
[46] E. Kozhevnikova, E. Rafiee, I. V. Kozhevnikov, *Appl. Catal. A Gen.* **2004**, *260*, 25–34.
[47] G. Sartori, R. Maggi, *Chem. Rev.* **2006**, *106*, 1077–1104.
[48] R. Lin, S. Mitchell, T. Netscher, J. Medlock, R. T. Stemmler, W. Bonrath, U. Létinois, J. Pérez-Ramírez, *Catal. Sci. Technol.* **2020**, *10*, 4282–4292.
[49] N. N. Duong, B. Wang, T. Sooknoi, S. P. Crossley, D. E. Resasco, *ChemSusChem* **2017**, *10*, 2823–2832.
[50] E. Kozhevnikova, J. Quartararo, I. V. Kozhevnikov, *Appl. Catal. A Gen.* **2003**, *245*, 69–78.
[51] G. D. Yadav, G. George, *J. Mol. Catal. A Chem.* **2008**, *292*, 54–61.
[52] M. G. Evans, M. Polanyi, *Trans. Faraday Soc.* **1935**, *31*, 875.
[53] A. D. Becke, *J. Chem. Phys.* **1993**, *98*, 5648–5652.
[54] M. J. Frisch, G. W. Trucks, H. B. Schlegel, G. E. Scuseria, M. A. Robb, J. R. Cheeseman, Gaussian09, Revision B.01, Gaussian Inc., Pittsburgh, PA, **2003**.

Manuscript received: July 9, 2025
Revised manuscript received: September 19, 2025
Accepted manuscript online: September 28, 2025
Version of record online: ■■, ■■